Zeolite Structure and Reactivity by Combined Quantum-Chemical−Classical Calculations

Alex H. de Vries,*,† Paul Sherwood,† Simon J. Collins,† Anthony M. Rigby,‡ Marcello Rigutto,‡ and Gert Jan Kramer‡

Department for Computation and Information, Daresbury Laboratory, Daresbury, Warrington WA4 4AD, United Kingdom, and SHELL International Oil Products, Badhuisweg 3, 1031 CM Amsterdam, The Netherlands

Received: April 20, 1999

Proton-energy differences, ammonia adsorption, and D/H-exchange barriers for methane at selected isolated Brønsted sites in zeolites FAU, MFI, BEA, ERI, and CHA are studied by combined quantum-chemical−classical (QM/MM) calculations in an attempt to understand the factors that determine the reactivity at these Brønsted sites. The barrier of the D/H-exchange reaction for methane was found to correlate well with the calculated ammonia chemisorption energy, but even better with the O−Al−O angle of the free zeolite Brønsted site the reaction is taking place on, provided the Si−O−Al−O−Si moiety over which the reaction takes place is more or less collinear. The barrier is considerably higher if this collinearity is weaker, which may be explained by the necessity of costly backbone distortions to accommodate the geometrical requirements of the transition state. This is confirmed by similarly strong correlations with the O−Al−O angle change going from the free acid site to zeolite−ammonium ion bidentate structures, which may be thought of as a measure of the backbone distortion. A new measurement of the D/H-exchange barrier in BEA is also reported. It was found to be 88 ± 18 kJ/mol, lower than the experimental barriers in both FAU and MFI.

Introduction

Zeolite-based acid catalysts are widely used in a number of commercially important petrochemical processes, including catalytic cracking, hydrocracking, and isomerization. They are particularly useful since they are solid, are thermally stable, and can have selectivities owing to their microporous structures. Their catalytic performance can often be improved by varying the properties of the acid sites or by choosing a different pore structure. An understanding of the processes within the zeolite and the way in which these are influenced by changes in the acid site or the pore structure, as well as the reacting hydrocarbons, would significantly assist efforts to improve existing catalysts and create new ones. Such an understanding cannot be obtained purely by experimental techniques because of the complex interplay between the many physical and chemical processes taking place in the zeolite, and computational chemistry has become established as a complementary technique in obtaining insight into the microscopic detail of the catalysis.[1]

There are two main streams of this research which address different aspects of the catalysis. The catalytic reactions themselves have been studied with quantum-chemical methods for small molecules on models of the active sites. The adsorption and transport of molecules through the zeolite lattice has been studied with molecular dynamics (MD) and Monte Carlo (MC) simulations with classical force fields.

This work provides valuable information but has its weaknesses. The force fields used in the classical studies cannot describe the catalytic reactions. This can be addressed by new force fields which are able to describe bond breaking and bond formation, but this requires extensive parametrization for each reaction and is therefore very laborious. The small model acid-site clusters used in the quantum-chemical calculations cannot distinguish fully between different acid sites (although acid-strength effects can be roughly modeled[2]). Important effects such as adsorbate−wall interactions and long-range electrostatics are neglected. This could be addressed by using larger clusters[3,4] or by including the full periodic system,[5] but these methods may become prohibitively expensive to use on a routine basis.

A third approach has been developed over the past two decades combining the advantages of the two approaches in a single calculation.[6−21] The portion of the system in which the reaction is taking place (the acid site and the reacting molecule) is modeled by quantum-chemical methods, and the rest of the system is treated with classical force fields. This allows for the inclusion of geometric and electrostatic effects of the rest of the lattice into quantum-chemical models of the catalytic reaction at little additional computational cost. Successful application of this method allows the modeling of differences between catalytic sites and between hydrocarbons.

The overall success of the method depends on accurately combining the two parts of the model. For example, the details of the force field are important (many give the correct overall properties of the zeolite but do not describe important local effects), as is the treatment of the QM/MM boundary region, where the boundary actually cuts through covalent Si−O bonds.

In this study, we aim to investigate whether this method can describe reactions in zeolites in a meaningful way. We have taken the methane−zeolite D/H-exchange reaction since this can be studied in detail experimentally and has been modeled using bare-cluster quantum-chemical methods. These bare-cluster calculations suggest that there is a correlation between the activation energy and the difference in proton affinity at the O-atoms involved in this exchange.[2] In these clusters, the

* To whom correspondence should be addressed. Present address: Theoretical Chemistry, Nijenborgh 4, 9747 AG Groningen, The Netherlands. E-mail: A.H.de.Vries@chem.rug.nl.

† Daresbury Laboratory.

‡ SHELL International Oil Products.

10.1021/jp9913012 CCC: $18.00
Published on Web 00/00/0000 PAGE EST: 8.9

proton affinity may be tuned by varying the length of the peripheral Si−H bonds. The geometry of the clusters used was not restrained to reflect the geometric constraint present in a real zeolite, say FAU or MFI.

In this paper, we explicitly calculate proton-energy differences and D/H-exchange barriers at specific Brønsted acid sites in different zeolites, taking into account their particular geometry. The nature of Brønsted acid sites was further investigated by the ammonia physisorption and chemisorption processes, and correlations were sought between the D/H-exchange barriers and the energies associated with zeolite−ammonia interactions. Strong correlations with acid-site geometry were not expected, mainly because of the smallness of methane and because of the bare-cluster results.

Experimental data on the D/H-exchange reaction[22] and ammonia sorption[23] are available for some zeolitic systems. Comparison to calculated values is not in general straightforward because the experimental systems are usually less well defined than the computational counterparts. Nevertheless, here we also comment on experimental data and our calculated values, and report a newly measured D/H-exchange barrier for zeolite BEA.

Method

Our combined quantum-chemical−classical (QM/MM) model will be presented in detail elsewhere, but the main features will be discussed briefly here.

QM/MM Cluster. The systems studied comprised of *finite* siliceous zeolite clusters of 35 bohr radius from a selected T-site, typically yielding 1000−1500 atoms. Only a single Al-for-Si substitution was made in the entire QM/MM cluster. This substituted site did not necessarily coincide with the center of the cluster, but was always in the central region. The zeolite starting coordinates were taken from crystal data of the siliceous structures.

QM Region. The QM region consisted of the zeolite acid site comprising five T-atoms and any substrate (ammonia, methane) if present. The central T-atom in the QM cluster is an Al, creating an acid site. The other four T-atoms are the ones connected to the O-atoms bonded to Al. All QM clusters in this study were Si−H terminated. Termination with H is part of the embedding procedure, serving to satisfy the valence of the Si−O σ-bonds that are cut across in defining QM and MM regions. The ab initio LCAO-MO wave function for the QM region was determined by the restricted Hartree−Fock self-consistent field (RHF-SCF) procedure. Geometry optimizations were done at the 3-21G level. Single-point energies at these geometries were calculated at the 6-31G* level. Some geometries were also optimized at the 6-31G* level; this never resulted in relative energy changes of more than 5 kJ/mol, except in the calculation of the sorption energy of NH_3 on an acid site. The reasons for this are discussed in the appropriate section.

MM Region. The MM region consists of all atoms that are not treated explicitly in the QM system. This includes the O-atoms bound to the QM Si-atoms. For the interaction between the MM atoms we used the aluminosilicate consistent force field (CFF) due to Hill and Sauer.[24] This force field consists of bond-stretch, angle-bend, torsion, and coupling terms, as well as an r^{-9} repulsive potential, all parameters being derived from quantum-chemical cluster calculations at the Hartree−Fock level. For electrostatic interactions through point charges at the MM atoms we do not use the CFF charges, however, but our own potential derived charges, which also serve to generate the potential included in the QM Hamiltonian (vide infra).

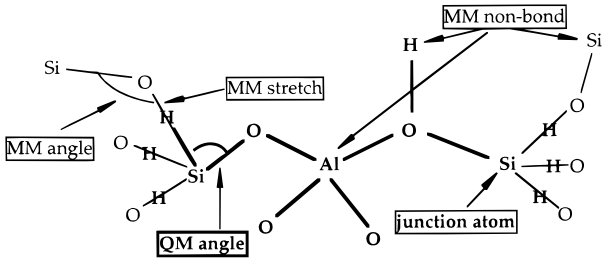

Figure 1. Hybrid QM/MM setup. Atoms in bold type are treated quantum mechanically. MM forces are added for stretching, bending, torsion, and nonbonded terms not within the QM system. Some examples are indicated in the figure. The junction-terminating H bond lengths are fixed, and the terminating H are constrained to lie along the QM/MM bond cut. A MM stretch term between the junction atoms and first MM atoms is added.

TABLE 1: Zeolite Framework−Substrate Nonbonded Interaction Parameters[a]

atom types	C6 (10^3 kJ bohr^6/mol)	C12 (10^6 kJ bohr^{12}/mol)
Si−H[b]	−93.3262	5486.9096
O−H[b]	−23.2010	567.4308
Si−C[b]	−165.8753	17914.5380
O−C[b]	−45.1360	2219.5637
Si−N[c]	−75.8737	4085.1858
O−N[c]	−80.0788	1526.5521

[a] Energy expression: $U_{ij} = C6_{ij}/r_{ij}^6 + C12_{ij}/r_{ij}^{12}$. [b] From Nicholas et al.[27] [c] From CHARMM recipe[28] with DRF FF parameters[19] (α_{Si} = 6.434, α_O = 6.074 Bohr^3 are taken from de Vos-Burghart et al.[54]).

QM/MM Mechanical Interactions. The setup and treatment of the QM/MM system for an acid site is illustrated in Figure 1. The QM fragment is defined as including the capping (or terminating) H-atoms which model the O-atoms bonded to the junction Si-atoms. The QM fragment is held within the entire cluster by the CFF mechanical forces: to the set of MM interactions are added those bend and torsion terms that involve both QM and MM atoms, except for the terms in which the only MM atom is the junction O. Thus, the angle bend O(QM)−Si(QM)−O(MM) is assumed to be described correctly by the QM O−Si−H force; the corresponding MM term is not present. (This bookkeeping approach contrasts with those models which attempt to correct for the approximation around the QM/MM junction by subtraction of a MM energy from the QM cluster, as in, e.g., refs 20, 21, and 25.) One exception is made to this rule: the junction-O(MM) stretches are described by the CFF terms, constraining the junction-H distances to a fixed length.

The rationale for constraining the junction-H distances to a fixed length is the need to define the H-positions from "real" atom positions for obtaining analytic gradients. Also, there is a proven sensitivity of the computed proton affinity of the acid-site structure to this junction-H bond length for smaller aluminosilicate clusters in the gas phase.[26] By fixing this distance across zeolites and acid sites, the comparison is believed to be unbiased, and any effect of varying this distance may be studied separately.

Nonbonded framework−hydrocarbon interaction parameters were taken from a molecular dynamics study of absorption of propane in all-silica zeolites by Nicholas et al.[27] This is an all-atom 6−12 Lennard-Jones potential. Nonbonded framework−N interaction parameters were generated by the CHARMM recipe for the repulsion,[28] and the Slater−Kirkwood formula for the dispersion, using the DRF force field parameters for N,[19] also yielding a 6−12 potential. For convenience, all nonbonded framework-substrate parameters are collected in Table 1.

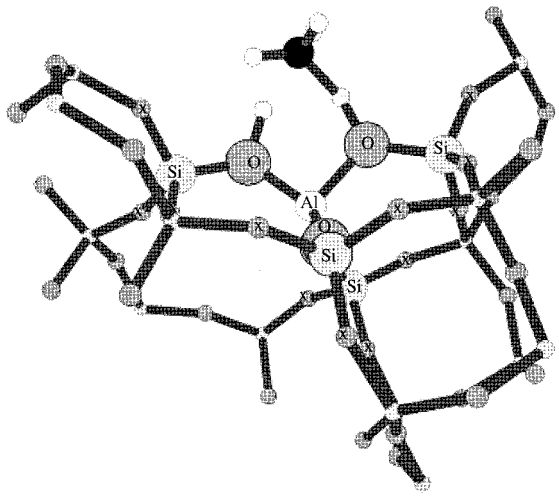

Figure 2. Moviemol[55] drawing of the QM/MM partitioning in FAU. Large atoms are in the quantum region, small atoms in the MM region. The atoms marked Si are H-terminated, with the H-atoms lying on the Si−O bonds. The O-atoms marked "x" are involved in this termination scheme. These O-atoms do not bear a charge, which is shifted to their MM Si neighbors. Note that only a small part of the MM region is shown.

QM/MM Electrostatic Interactions. All results presented here pertain to the electrostatic embedding level, as described by, e.g., Bakowies and Thiel.[20] This means the QM cluster is not only embedded in the mechanical potential of its surroundings, but the electrostatic potential due to its surroundings are added to the Hamiltonian and treated self-consistently in the HF-SCF approach. The electrostatic potential added to the QM Hamiltonian was generated by our generic zeolite point-charge model,[29] with Si−O bond contributions[24] of ±0.30 electron, rather than the CFF value (±0.13*e*). This model was derived from the fitting of charges at the nuclei to reproduce the computed periodic Hartree−Fock potential for a range of zeolitic structures. We have checked the structural stability of our clusters with our model charges and do not observe drastic differences in behavior as may be expected from a valence force field.

Overall neutrality of the embedding model is assured by using bond contributions, i.e., an O-atom at the cluster edge connected to one Si only, is given a charge of −0.3*e*, rather than −0.6*e*, which it would have if it was connected to two Si-atoms; only partly connected Si-atoms are treated likewise. Fourteen point charges on the edges and faces of a cube surrounding the MM cluster were added in order to best reproduce the *periodic* potential in the region of the active site with a finite MM cluster. The periodic potential to be reproduced corresponds to that in a fully siliceous structure in which the Si- and O-atoms bear our potential-derived charges (Si, +1.2*e*; O, −0.6 *e*).

To avoid spurious QM polarization, residual charges on O-atoms bonded to junction Si-atoms were shifted to their nearest MM neighbor. A dipole compensating for this charge shift was introduced at that same neighbor.

An example of the QM/MM partitioning is given for the D/H-exchange reaction in FAU in Figure 2. Note that only a small part of the MM region is shown for reasons of clarity. The entire QM/MM cluster in this case comprises of 1054 atoms.

Geometry Optimization. Geometry optimizations (minimization and transition-state (TS) searching) were performed in mixed Cartesian-*z*-matrix (internal) coordinates, without imposing any symmetry restrictions. Geometry optimization of the QM/MM cluster was never allowed in full, but only for atoms up to five bonds removed from the central Al; the outer parts were always kept fixed. Minimizations and TS searches were performed with modified Baker eigenvector-following algorithms,[30] with the hybrid Murtagh-Sargent/Powell update of the Hessian.[31] The optimization algorithms and the QM/MM interfacing were implemented in ChemShell,[32] under development at Daresbury Laboratory. GAMESS−UK[33] was used for calculation of energy and gradient of the QM part, and for the MM part appropriate routines for energy and gradient calculations were taken from the DL-POLY package,[34] with some modifications to accommodate the CFF force field.

TABLE 2: Relative Proton Energies (kJ/mol) on Selected Zeolite Brønsted Acid Sites[a]

		ΔE_{rel}	
zeolite	O-site	3-21G	6-31G*[b]
FAU	O1	0	1 (2)
	O2	30	12 (10)
	O3	18	0 (0)
	O4	17	14 (14)
MFI T2	O1	8	6 (7)
	O2	0	0 (0)
	O6	39	21 (20)
	O13	95	77 (68)
MFI T3	O2	0	2
	O19	44	20
	O20	0	0
MFI T6	O5	4	2
	O18	0	0
	O19	57	36
MFI T7	O7	12	7
	O17	14	9
	O22	0	0
	O23	4	1
BEA T5	O5	0	0
	O9	0	1
ERI T1	O1	0	0 (0)
	O4	5	5 (2)
CHA	O2	2	5 (3)
	O3	0	0 (0)

[a] Nomenclature of the sites according to crystal structure data as referenced in the text. [b] Values in parentheses denote geometry-optimized results.

Experiment. Rates of the hydrogen−deuterium exchange reaction betweeen deuteriomethane and Brønsted acid hydroxyl groups of zeolite beta (BEA) were measured at 623, 673, and 723 K at a deuteriomethane pressure of 1.73 kPa (13 Torr), using infrared spectroscopy as described in an earlier paper.[22]

Results and Discussion

Brønsted Acid Sites. The relative proton energies of a number of Brønsted acid sites in the zeolite structures of FAU, MFI, BEA, ERI, and CHA are collected in Table 2. In FAU[35] and CHA[36] there is only one crystallographically unique T-site to be substituted. In MFI[37] there are 12 such sites. We have investigated sites T2, T3, T6, and T7, using the numbering convention of Olson et al.[38] In BEA[39] we have looked at site T5 only; in ERI[40] we have studied site T1 only. We give relative proton energies at a particular site only, i.e., the energies of moving a proton from being attached to one O to another, with the same siting of the Al. Deprotonation would result in a charged Brønsted site embedded in a potential which has an offset consistent with the Ewald surface of the periodic system, and the energy is therefore difficult to compare between different zeolites. Experimental deprotonation energies are not measured directly, but are derived from O−H vibrational shifts upon absorption of a weak base.[41] It is not our aim here to derive

absolute deprotonation energies, nor to compare the relative stabilities of different Al sitings within a given zeolite, although such comparisons may be made within our methodology by enlarging the QM cluster to span a number of Al sites of interest.

The relative proton energies at a site calculated by our method (Table 2) are seen to be quite sensitive to the basis set used. The width of the distribution at each site is considerably lower at the 6-31G* level. With the larger basis set the relative stability of certain sites also changes. The most striking example of this is FAU, where only at the 6-31G* level the O3-site is predicted to be the most stable, in agreement with experiment.[42] Interestingly, we find the O1-site in FAU very close in energy to the O3-site, closer than in any previous computational study.[26,43−45] The energy difference found here (1 kJ/mol) is in complete agreement with the experimental difference calculated from relative occupancy.

Comparing our results in MFI to previous force field studies, again we find a much smaller width of the energy distribution on each site than Kramer and van Santen,[26] if we discount the sites with protons pointing into small cages. These sites are found here at higher energies than in that study, which may be explained by the fact that in the force field study no explicit H-atoms were used, but effective O−H groups, thereby ignoring specific H−zeolite repulsion. The width of the distributions we find is closer to that found in the force field study by Schröder et al.,[46] although differences in the relative stability of the sites occur frequently. Experiments show a broadened O−H band in the infrared, not in conflict with a distribution of protons over a number of different sites, as argued by Schröder et al.

Ammonia Sorption. The failure to calculate absolute proton affinities for our embedded clusters leaves a problem with the comparison between acid sites within different zeolites. The acid-site strength is a hotly debated property, especially as it may be a useful quantity in predicting catalytic activity.[41] For the D/H-exchange reaction, the relative proton energies of the participating O-sites, rather than the absolute proton affinities, has been found to correlate to the barrier in QM cluster calculations.[2] Nevertheless, one would like to establish a measure of acidity. We have investigated the proton-transfer energy to convert ammonia in the physisorbed state to a chemisorbed ammonium ion as well as the ammonia chemisorption energy. The latter suffers from an incomplete description in the sense that at the HF level electron correlation is ignored, and therefore the dispersion interaction between the ammonia or ammonium ion and the QM part of the backbone is not included. Also, the values we report are not corrected for basis-set extension effects. Both errors are assumed to cancel in comparing the physisorbed and chemisorbed species.

In all cases, the chemisorbed species were found to have bidentate structures. Local minima for the physisorbed species were sometimes difficult to find, and we have chosen to define a physisorbed state by restraining the O−H distance to be the value in the free Brønsted acid. The proton-transfer and chemisorption energies for selected sites are given in Table 3.

The proton-transfer energies between physisorbed ammonia on the Brønsted acid sites and bidentate chemisorbed ammonia provide us with a way to distinguish between different Brønsted sites. Excepting the T1-site in ERI, the proton-transfer energies span a range of ca. 20 kJ/mol, with an approximate basis-set effect of −10 kJ/mol going from the 3-21G to the 6-31G* level. In accord with all studies to date that include the electrostatic field of the lattice, we find the chemisorbed bidentate ammonium species to be more stable than the physisorbed ammonia species. The proton-transfer energies correspond quite well to the embedded cluster calculations by Greatbanks et al.,[47] being of the order of 10 kJ/mol for the larger basis set. The monodentate ammonium species, which have been studied extensively in both bare[3,47,48] and embedded cluster,[5,49,50] and periodic[51] approaches, are the subject of a separate study and will not be discussed here. The reason for choosing the bidentate structures is the hope that the commonality of structure between the bidentate ammonium species and the D/H-exchange transition-state structure will make the properties of the ammonium species a good predictor for the D/H-exchange barriers.

TABLE 3: Ammonia Chemisorption Energy and $H_3N\cdots HOZ \rightarrow H_3NH\cdots OZ$ Transfer Energy (kJ/mol) at Selected Zeolite Brønsted Acid Sites

		$\Delta E_{chemisorption}$		$\Delta E_{transfer}$	
zeolite	O-site[a]	3-21G	6-31G*	3-21G	6-31G*
FAU	O1 (O4)	151	73 (86)	20	15 (18)
	O4 (O2)	127	75	34	1
MFI T2	O2 (O1)	152	91	24	10
	O2 (O6)[b]	129	98	1	17
MFI T3	O2 (O20)	158	101	28	17
MFI T6	O18 (O5)	148	101	28	14
MFI T7	O22 (O7)	153	99	15	1
	O23 (O17)	160	110	24	17
BEA T5	O5 (O9)	160	88	28	10
ERI T1	O1 (O4)	87	37	−5	−28
CHA	O3 (O2)	135	68 (78)	22	6 (11)

[a] The first O-site listed bears the acidic proton in the physisorbed species; the second O-site is the site with which the ammonia forms the other H-bond. [b] Physisorbed species is $O(2)—H\cdots NH_3$ (O(1)).

At the T1-site in ERI, we find the physisorbed species to be more stable than the bidentate chemisorbed species. This may be explained by the fact that the rings in ERI are the smallest studied, viz. 8-rings, which causes the bidentate bonding mode to introduce considerable strain in the backbone, because in order to interact with both hydrogens, the Si−O−Al−O−Si moiety involved should be as collinear as possible. Similarly, in CHA, which also has 8-rings, the chemisorbed species is only slightly more stable than the physisorbed species. The deformation effect also plays a role in the TS of the D/H-exchange reaction, and is discussed in more detail below.

Reliable experimental values for heats of ammonia chemisorption on Brønsted sites of zeolites are scarce, mainly because most measurements have been performed either on impure materials (containing Lewis acid sites that are known to bind such bases preferentially) or at too low temperatures. Parillo et al. [23] did careful calorimetric experiments on well-characterized materials and reported values of 150 kJ/mol for H−ZSM-5 and coverage-dependent values ranging from 150 to 120 kJ/mol for a high-silica zeolite Y material. The zeolite Y sample that was used contained extraframework aluminum, for which reason it is likely that the low-coverage value of 150 kJ/mol contains a contribution from interaction with Lewis acid sites and should be somewhat lower for a pure material.

The relative calculated values for MFI and FAU (18−28 kJ/mol at the 6-31G* level, Table 3) agrees well with the observed difference of 0−30 kJ/mol. The absolute calculated values appear to be too low. The deficiencies in the theoretical description mentioned earlier may account largely for this observation. Greatbanks et al.[50] observed a correlation effect of 35 kJ/mol for their embedded clusters at the MP2/6-31G** level. Considering our QM cluster is larger than theirs, chemisorption energies would be at least 130 kJ/mol in MFI, which is quite close to the experimental value.

The basis-set superposition error (BSSE) again decreases the chemisorption energy. We have calculated this with the standard

TABLE 4: Calculated and Experimental D/H-Exchange Barriers (kJ/mol) in Methane at Selected Zeolite Brønsted Acid Sites

		ΔE_{act}		
zeolite	O-sites[a]	3-21G	6-31G*[b]	expt
FAU	O1−O4	186	261 (262)[b]	129 ± 20
	O4−O2	213	271	
MFI T2	O2−O1	184	250	
	O2−O6	240	291	
MFI T3	O2−O20	182	248	109 ± 15
MFI T6	O18−O5	189	254	
MFI T7	O22−O7	191	247	
	O23−O17	187	246	
BEA T5	O5−O9	180	249	88 ± 18
ERI T1	O1−O4	209	267	
CHA	O3−O2	189	258	

[a] The O-sites listed denote the O-atoms with which the H−C−H moiety forms a bridge in the TS structure. The activation barrier is measured from the minimum with the acidic proton on the first O-site listed. [b] Value in parentheses denotes geometry-optimized results.

counterpoise method and found it to be 8 kJ/mol in FAU, similar to that found by Greatbanks et al.[50] of 6−10 kJ/mol. There is another basis-set effect, a basis-set extension effect (BSEE), however, in these calculations which *increases* the sorption energies, as can be seen from Table 3. The chemisorption energies in FAU and CHA have been recalculated at level of geometrical relaxation in the 6-31G* basis set. They are increased by ca. 15 kJ/mol. This is a consequence of the relaxation energy (from the 3-21G-optimized geometry) of the zeolite anion−ammonium ion complex being considerably larger (ca. 35 kJ/mol) than that of the free acid site (15 kJ/mol) and ammonia (5 kJ/mol). Relaxing the free acid site in CHA in the presence of the ammonia basis functions (at the 3-21G-optimized geometry, also with ammonia basis functions present) results in an acid-site relaxation energy of 6 kJ/mol. Accounting for this effect, the statement that using 6-31G* results at 3-21G-optimized geometries is sufficient for the type of analysis we perform in this paper is confirmed. Note that the transfer energy of the proton from the acid site to the ammonia changes by only 3 kJ/mol when allowing 6-31G* geometry relaxation (Table 3).

D/H-Exchange Barriers. D/H-exchange barriers for this reaction at selected sites are given in Table 4. The barriers are given with respect to the lowest minimum, which is a methane molecule adsorbed on the Brønsted acid site. The O-atoms involved in the exchange are indicated in the Table. Figure 3 shows plots relating the barriers to the proton-energy difference of the participating O-atoms at the 3-21G and 6-31G* levels.

The transition state for the D/H-exchange between a zeolite Brønsted site and an alkane (in our case methane) has been characterized as being of a covalent nature, judged by geometry and Mulliken overlap population analysis resulting in an apparent coupling of the barrier to the relative energies of reactant and product, which is indeed observed in the bare-cluster calculations.[2]

Electronic Properties of Brønsted Site. In the embedded-cluster calculations there is no clear overall correlation between the proton-energy differences and the barriers (Figure 3), in marked contrast to the above-mentioned cluster calculations, although the electronic structures of the minima and TS's are very similar in the bare-cluster and embedded calculations. In the embedded calculations, the electronic properties of the QM cluster are influenced by both the geometric distortions and the electrostatic field of the surroundings. In the bare-cluster calculations, the electronic properties of the cluster are influenced strongly by the peripheral Si−H bond lengths. Thus, the relative proton affinities of the O-sites in bare and embedded clusters are brought about in a different manner. The effect of changing the peripheral Si−H bond lengths on the proton energies and D/H-exchange barriers found in the bare clusters is found to persist in the embedded calculations. This is shown in Table 5 for the MFI T7 zigzag channel site. All structures were reoptimized, but the geometrical changes were very small on changing the Si−H bond lengths.

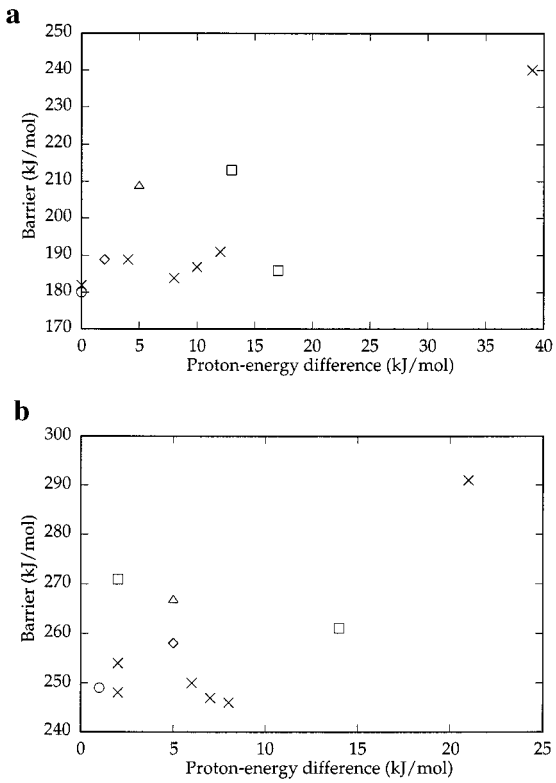

Figure 3. D/H-exchange barrier vs proton-energy difference plot. (a) HF/3-21G level; (b) HF/6-31G*//3-21G level. □, FAU; ×, MFI; ○, BEA; △, ERI; ◇, CHA.

TABLE 5: Proton-Energy Difference Energies and D/H-Exchange Barriers in Methane at MFI T7 (Zigzag channel) Site as a Function of Si−H Junction Bond Lengths

		$\Delta\Delta E_{proton}$ (kJ/mol)		ΔE_{act} (kJ/mol)	
junction	Si−H (Å)	3-21G	6-31G*	3-21G	6-31G*
all	1.6	9	7	186	241
all	1.5	10	8	187	246
all	1.4	10	9	186	250
Si17	1.6				
Si23	1.4	27	26	195	255
Si7, Si21	1.5				
Si17	1.4				
Si23	1.6	−7	−10	178	238
Si7, Si21	1.5				

A number of variations were made in the Si−H distances. First, *all* Si−H distances were varied in the same way. This changes the absolute proton affinities but hardly affects the relative proton energies of O23 and O17. This uniform change in Si−H distance across the whole embedded cluster influences the results at the 6-31G* level in a fashion similar to the bare-cluster calculations, be it a bit stronger. Second, only the Si−H distances on the Si-atoms bound to the O-atoms involved in the exchange reaction were varied, increasing one distance while reducing the other. It is clear from Table 5 that there is a strong influence of the Si−H bond lengths on the calculated relative

proton energies and D/H-exchange barriers when changing them differentially across the embedded QM cluster, as was found in bare-cluster calculations.

To assess the importance of this effect in accurate modeling of real zeolites, one has to address two questions:

1. Does the changing of the peripheral Si−H bond lengths convey a real effect present in zeolites? It has been argued that tuning the Si−H distances models the electronic changes upon changes in Si−O bond lengths present in the real zeolite. This may be tested by recalculating the processes with larger QM clusters which include the Si−O moieties involved.

2. Is the variation in Si−O bond lengths at particular sites large enough to warrant the modeling by differential peripheral Si−H bond lengths? For the sites studied here, the peripheral Si−O bond lengths in both experimental and optimized structures span a range of only 0.15 bohr over all sites in all zeolites, and a maximum 0.1 bohr at a given site. Given the effect on the barrier is 17 kJ/mol over a differential Si−H distance of 0.4 bohr, the attenuation of the results by establishing a coupling between the Si−O and Si−H distances is expected to be no more than 5 kJ/mol at the 6-31G* level (under the assumption that the Si−H length is to vary identically as the Si−O length from their respective equilibrium values), which is distinctly less than the observed span of the barriers of 20 kJ/mol due to purely geometrical and electrostatic factors.

One may conclude that the differential proton stabilities at the different oxygens caused by the geometric and electrostatic factors through the embedding is enough to distinguish between zeolitic Brønsted sites, and that additional attenuation of the QM cluster properties through varying peripheral bond lengths will not lead to results that differ significantly from the results obtained with the present embedding scheme.

Correlations of D/H-Exchange Barrier with Brønsted Site Properties. In the rest of this section we will focus on finding correlations between zeolite Brønsted site properties and the D/H-exchange barriers in order to gain insight into the catalytic nature of zeolitic sites. Figure 3 shows plots relating the barriers to the proton-energy difference of the participating O-atoms at the 3-21G and 6-31G* levels. At the 6-31G* level, a rough relationship between proton-energy differences and barriers may be observed going from one zeolite to the next (with the exception of ERI), with the barrier increasing with increasing proton-energy difference.

The D/H-exchange barriers between O2−O4 in FAU and O2−O6 at T2 in MFI (at 271 and 291 kJ/mol, respectively) were found to be considerably higher than the others. The reason for this is that in order for the exchange to take place in a concerted manner, the incoming and outgoing hydrogens need to interact with both the zeolite backbone oxygen and the methane carbon. To this end, the zeolite backbone needs to undergo considerable distortion if the Si−O−Al−O−Si moiety involved in the exchange is not more or less collinear in the reactant (free acid). The two TS's with high barriers do not fulfill this collinearity criterion. This is illustrated in Figure 4 for the reaction between O2−O6 at T2 in MFI. Figure 4a shows the relevant part of the TS structure for the exchange involving O1 and O2. It is seen that the Si3−O2−Al2−O1−Si1 moiety is almost collinear. In the exchange involving O2 and O6, shown in Figure 4b, the Si−O−Al−O−Si moiety bends around by approximately 120°, as measured by the Si3−O2−O6−Si6 torsion angle.

The energy increase in barrier on selecting a noncollinear arrangement at the T2-site in MFI corresponds to the deformation energy of the free MFI acid site at T2 from the relaxed

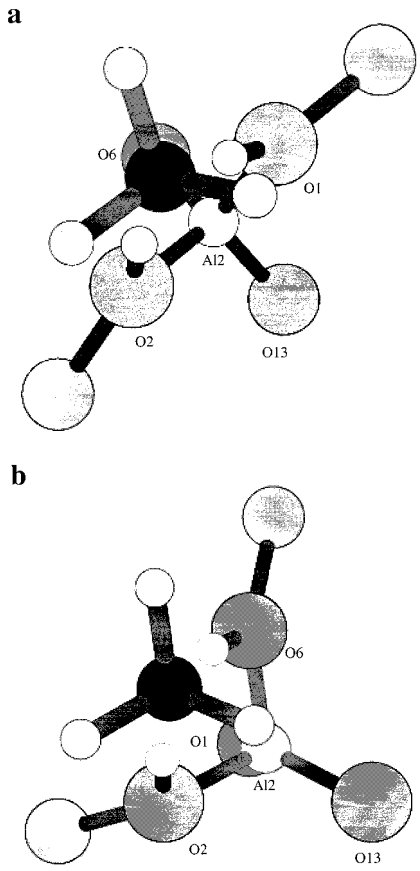

Figure 4. Moviemol[55] drawings of D/H-exchange TS's at the MFI T2 site. (a) O1−O2; (b) O2−O6. The labeling of the zeolite atoms is according to Olson et al.[38]

structure to the backbone structure in the TS, maintaining the free-acid O2−H distance. We expect the same effect for the O2−O4 barrier in FAU. Of course, interaction with methane may alleviate the energy cost of the distortion, but a reaction path that does not necessitate such a backbone distortion will be favored over one that does. One may conclude that only backbone fragments with the required collinearity are to be considered when calculating these barriers. These type of fragments are available in most zeolites. In MFI, only at T5 can such an arrangement not be found. On inspection, all other T-sites in MFI have one favorable pathway, except T7, where there are two possibilities: one where the adsorbate is in the straight channel and one where it occupies the zigzag channel. In extracting a rate for the overall D/H-exchange process by thermodynamic averaging,[2] one would need to take this observation into account and reduce the weight of the unfavorable pathways.

The high barrier in ERI may also be explained by this mechanism. No really favorable Si−O−Al−O−Si moieties appear to be available. Certainly, the site we have chosen is not ideal, but seems to be among the best available by inspection of the crystal structure. The results in ERI could be questioned with respect to the appropriateness of the QM/MM model. The ring is quite small and there may be interactions between the sorbate and the zeolite wall that should be treated by quantum mechanics. We have calculated the barrier including the full 8-ring in the QM region. The barrier at the 3-21G level is then 208 kJ/mol, compared to 209 kJ/mol with the standard T5 cluster. Together with the fact that the closest H−zeolite wall distance is 2.5 Å, we feel it is safe to use the standard approach.

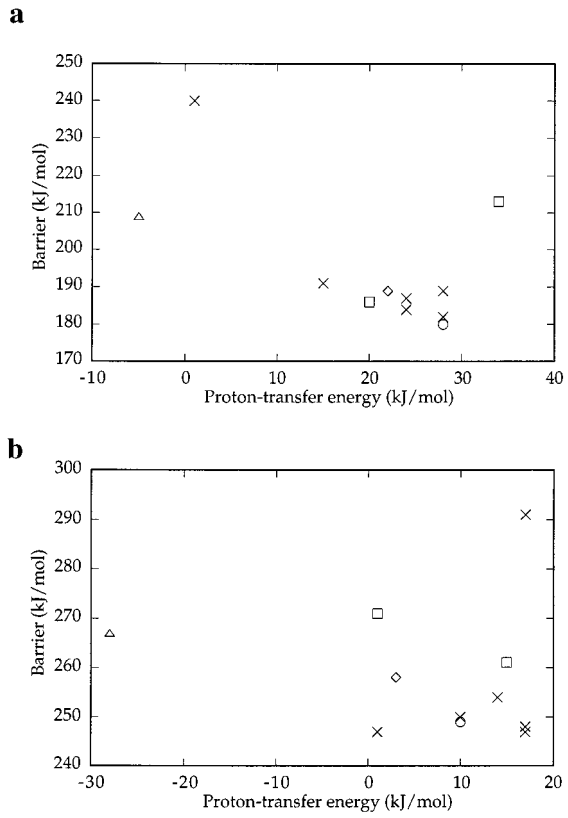

Figure 5. D/H-exchange barrier vs ZOH···NH_3—ZO···HNH_3 proton-transfer energy plot. (a) HF/3-21G level; (b) HF/6-31G* level. □, FAU; ×, MFI; ○, BEA; △, ERI; ◇, CHA.

Figure 5 shows the correlation between zeolite···ammonia—ammonium proton-transfer energies and the D/H-exchange barriers. Again, there is no clear relationship. Kramer and van Santen found only a weak dependence of the barrier on the proton affinity of the bare cluster. If the proton-transfer energy is a good measure of the acidity of a site, there is no apparent relationship between the acidity and the D/H-exchange barrier. The choice of the bidentate structure as the chemisorbed species may weaken the proton transfer as a measure of acid strength, as the bidentate nature may involve effects not involved in the "intrinsic" acidity of a site. Also, part of the acidity effect is lost in looking at the proton-transfer process, viz. the part which is present in the physisorption process with strongly interacting species, such as the ammonia molecule. Calculation of O—H frequency shifts upon adsorption of small molecules (N_2, CO) are expected to yield a better measure of the acidity.[41] However, one may expect the rearrangements from a physisorbed to the bidentate chemisorbed species to be a particularly useful measure for elucidating the particular D/H-exchange process, because of the similarity of the structures involved in both processes.

Interestingly, a reasonable to good correlation was found between the ammonia *chemisorption* energy and the D/H-exchange barrier at the 6-31G* level. This is shown in Figure 6. A linear fit had a regression coefficient (R^2) of 0.83. The fit can be improved if the barrier at the T6-site in MFI is discarded; the linear fit now has a regression coefficient of 0.92. There is good reason to exclude this point from the fit. The minimum structure at the T6-site is different from the other minima in that the methane molecule has moved considerably into the pore region of the zeolite and does not remain over the acid site as much as it does in the other minima. If the energy gained from this movement is of the order of 5 kJ/mol, the barrier at this

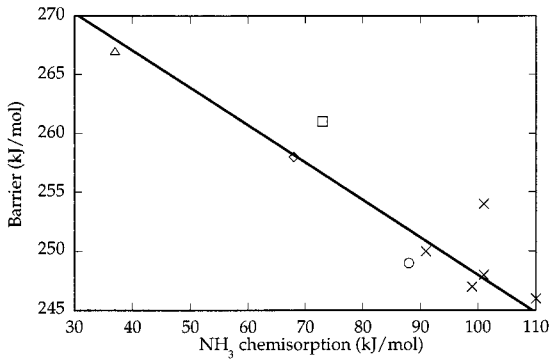

Figure 6. D/H-exchange barrier vs NH_3 chemisorption energy plot (HF/6-31G*//3-21G level). □, FAU; ×, MFI; ○, BEA; △, ERI; ◇, CHA. The line shows the linear fit ($R^2 = 0.92$) to the data excluding the barrier at the MFI T6 site (calculated barrier 254 kJ/mol).

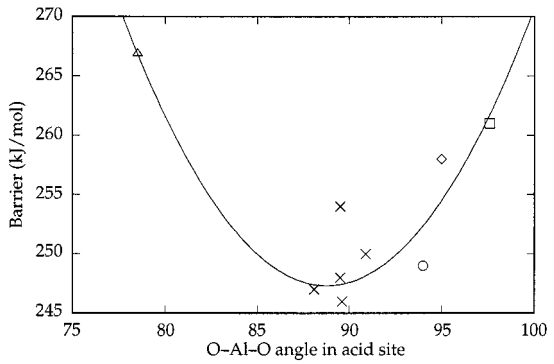

Figure 7. D/H-exchange barrier vs zeolite acid site O—Al—O angle plot (HF/6-31G*//3-21G level). □, FAU; ×, MFI; ○, BEA; △, ERI; ◇, CHA. The curve shows the quadratic fit ($R^2 = 0.93$) to the data excluding the barrier at the MFI T6 site (calculated barrier 254 kJ/mol).

site would become comparable to the other barriers, viz. 246—250 kJ/mol. An energy difference of 7 kJ/mol was found at the MFI T2-site when the methane molecule moved into the pore, being minimized from the O2—O6 TS to form methane + Z—O2—H, rather than from the O2—O1 TS, where the methane adsorbed with a C—H bond pointing to O1. We therefore feel that there is good reason to attach less weight in the correlation to the barrier at the T6-site in MFI as calculated.

We suggest here that the local geometry of the acid sites provides a useful handle on understanding the D/H-exchange barriers. Regression coefficients of quadratic fits of the barriers with the O—Al—O angle (1) in the free acid, (2) in the zeolite—ammonium ion complex, and (3) with the *change* in this angle going from the free acid to the chemisorbed ammonia were found to be high: $R^2 = 0.93$, 0.86, and 0.90, respectively. The correlation between the barrier and the O—Al—O angle in the free acid is shown in Figure 7. The plot suggests two aspects of the barrier. The first is the fact that there is an *optimum condition* for the reaction; the second is that geometrical factors are important. Note that the angles in BEA are in the same region as MFI, rather than FAU, despite the fact that BEA and FAU both have 12-rings. Fits of the barriers with acid-site width and height (defined by the Si—Si distances around the Al) proved too low to be useful in predicting the barriers (the best regression coefficient was 0.75).

The correlation of the D/H-exchange barriers with the ammonia chemisorption energy (Figure 6) may be explained by the similarity between the ammonium bidentate structure and the D/H-exhange TS structure, which also requires a bidentate orientation. Figure 8 shows the correlation between the ammonia

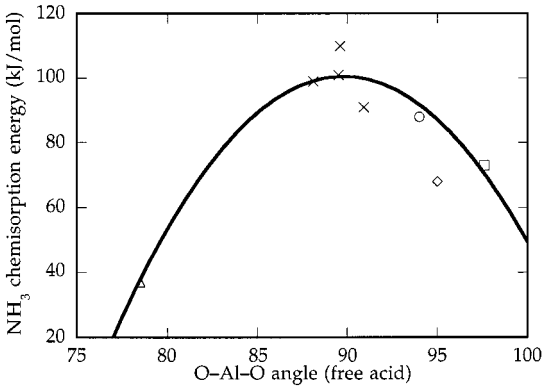

Figure 8. Ammonia chemisorption energy (kJ/mol) vs zeolite acid site O−Al−O angle plot (HF/6-31G*//3-21G level). □, FAU; ×, MFI; ○, BEA; △, ERI; ◇, CHA. The curve shows the quadratic fit (R^2 = 0.95) to the data.

chemisorption energy and the O−Al−O angle in the free acid for the different zeolites. Again, an excellent correlation is found (R^2 = 0.95) for a quadratic fit mirroring the fit for the D/H-exchange barrier. Although the interpretation of the ammonia chemisorption energy as a measure of acidity is not straightforward, the amminum bidentate structure may be regarded as a valuable model for the D/H-exchange TS structure.

The observed correlations may be interpreted as giving a dominant role to the local geometry of the Brønsted site. A possible added influence may be the wall−substrate interactions, but for this small hydrocarbon this is not expected to be as important. Indeed, the calculated embedded D/H-exchange barriers are very close to bare-cluster barriers reported in the literature.[2]

A much larger effect of local geometry deformation on the barrier was found in another hydrocarbon conversion reaction currently studied,[52] viz. the methyl shift reaction in a propenium ion adsorbed on an acid site. In that reaction, the TS is a formal cyclopropenium ion without apparent covalent bonding to the formally negative charged Brønsted site. The minimum there is not a physisorbed species, but a covalently bound propoxide species. Analysis of the contributions to the barrier in FAU showed a large differential effect of the backbone deformation necessary to accommodate the TS and minima, the minima being sterically less favorable because of the close zeolite wall−hydrocarbon contacts, bringing the barrier down by more than 70 kJ/mol with respect to bare-cluster calculations.[53] Most hydrocarbon conversion reactions are found to be of this type, viz. with a (formally) ionic TS, rather than a covalent one, and forthcoming work will concentrate on those reactions.

The computational study of the D/H-exchange reaction in larger hydrocarbons adsorbed on the Brønsted site will also have to address the consequences of the wall−substrate interactions, as they are expected to play an important role in overall reactivity. A combination of embedded QM cluster calculations on a limited number of conformations with classical MC or MD search techniques for favorable conformations may be the most efficient way to deal with those systems.[9]

The calculated barriers are too high in comparison with experimental values. The theoretical level at which the barriers are calculated here is not that high. In particular, electron correlation is absent. A first estimate of this contribution by adding the MP2 correlation energy difference between reactant and TS in the 6-31G** basis set (note there are polarization functions on H as well) at the 3-21G geometries indicates a dropping of the barriers by as much as 90 kJ/mol at T2 in MFI and 86 kJ/mol in FAU, bringing the barriers down to ca. 160 kJ/mol and 175 kJ/mol, respectively, in much closer agreement with experiment.

Calculations and Experiment. Comparing the relative height of the barriers in FAU, MFI, and BEA from theory and experiment (Table 4), it is seen that the calculations are only roughly corroborating with experimental data. The barriers in MFI and BEA are predicted and found to be considerably lower than in FAU, but whereas our calculations predict the barrier in BEA to correspond roughly to that in MFI, it is found to be lower still under experimental conditions. This discrepancy may be because we have picked a site in BEA that is not the most favorable, but further study of the sensitivity to the computational details is also required.

Conclusion

The newly developed combined quantum-chemical/force-field methodology has been applied to the study of the acid strengths of, and the methane D/H-exchange reaction on, several acid sites in various zeolitic structures.

The acid strength was characterized by the calculated ammonia chemisorption energies. Bidentate chemisorbed ammonium ion structures were found to be the most stable species in all but one case. It was found that the acid strength thus defined correlated well with fits to the local geometry of the site, particularly the O−Al−O angle in the free acid. The D/H-exchange barrier showed similar correlations, suggesting the local geometry of the sites is the dominant factor in determining this barrier. Correlation to proton-energy differences at the O-sites involved in the exchange reaction was not found to be good, in contrast to the results from bare-cluster calculations. In the embedded calculations, the electronic structure of the QM system is altered by interaction with the surrounding lattice and the geometry of the cluster, rather than by the change in peripheral Si−H bonds.

The chemisorption energy of ammonia was found to provide a reasonable linear correlation with the D/H-exchange barrier, suggesting the ammonium bidentate chemisorbed species provides a good model for the D/H-exchange TS, but the best correlation is with the local geometry of the Brønsted site and the distortion necessary to accommodate the TS. It appears that a O−Al−O angle of 94−98° in combination with a collinear Si−O−Al−O−Si moiety is optimal for this reaction. This study shows that 10-rings (MFI) are best suited to provide this geometry. If the constraints of the zeolite lattice favor either a smaller (ERI, CHA, 8-ring) or larger (FAU, 12-ring) O−Al−O angle, the barrier increases owing to backbone rearrangements. BEA seems to be an exception to the 10-ring rule, with a relatively small barrier despite having 12-rings. The O−Al−O angle in BEA is close to those found in MFI, however, and it is this measure that gives the best correlation with the barriers. The importance of local distortions in determining the barrier is also found for D/H-exchange processes along "bent" Si−O−Al−O−Si moieties, as was shown for both FAU and MFI. This has implications for thermodynamic weighting of possible reaction paths.

The agreement with experimental measures, including relative occupation of the O-sites in the free acid, ammonia chemisorption energies, and D/H-exchange barriers is encouraging, but further study of the peculiarities of the embedding remains necessary, especially if a direct connection to experiment is to be made. The compatibility of the force field with the QM level of approximation, the accuracy and transferability of point-charge representations used to emulate the electrostatic field at the reaction site, and the treatment of the QM/MM boundary

are some of the issues that may be crucial to obtaining quantitative results.

The statistics on which these conclusions are based may be considered poor, especially for the quadratic correlation with O−Al−O angle, as there are no data between angles of 79 and 87°. Nevertheless we feel the conclusion that the local geometry of the Brønsted site is the most important factor in determining the intrinsic barrier is well founded. Comparison to experiment is not as straightforward as it may seem. Questions arise as to the reference point in experiment (methane in the gas phase or adsorbed in the zeolite), the sites at which the reaction takes place, the importance of describing zeolite−methane dispersion interactions accurately (stepping up to the MP2 level for the QM region and testing the accuracy of the 6−12 potential), influence of MM polarization, as calculated with reaction field models[17] or shell-model potentials,[45] and the amount of geometrical zeolite lattice relaxation to be included.

In summary, this study has shown that the combined QM/MM methods can be used to describe the differences in strength between the different sites, can model the influence of geometrical constraints on the transition states, and can be used in conjunction with effective algorithms for the location of transition states without imposing symmetry constraints at little additional cost over bare-cluster calculations.

Acknowledgment. A.H.V. thanks SIOP Amsterdam for funding an extended visit and CPU time on their IBM SP2.

References and Notes

(1) Catlow, C. R. A. *Modeling of structure and reactivity in zeolites*; Academic Press: London, 1992.
(2) Kramer, G. J.; Santen, R. A. van. *J. Am. Chem. Soc.* **1995**, *117*, 1766.
(3) Brand, H. V.; Curtiss, L. A.; Iton, L. E. *J. Phys. Chem.* **1992**, *96*, 7725.
(4) Brand, H. V.; Curtiss, L. A.; Iton, L. E. *J. Phys. Chem.* **1993**, *97*, 12773.
(5) Teunissen, E. H.; Jansen, A. P. J.; Santen, R. A. van; Orlando, R.; Dovesi, R. *J. Chem. Phys.* **1994**, *101*, 5865.
(6) Warshel, A.; Levitt, M. *J. Mol. Biol.* **1976**, *103*, 227.
(7) Thole, B. T.; Duijnen, P. Th. van. *Theor. Chim. Acta* **1980**, *55*, 307.
(8) Singh, U. C.; Kollman, P. A. *J. Comput. Chem.* **1986**, *7*, 718.
(9) Field, M. J.; Bash, P. A.; Karplus, M. *J. Comput. Chem.* **1990**, *11*, 700.
(10) Gao, J.; Xia, X. *Science* **1992**, *258*, 631.
(11) Vasilyev, V. V.; Bliznyuk, A. A.; Voityuk, A. A. *Int. J. Quantum Chem.* **1992**, *44*, 897.
(12) Luzhkov, V.; Warshel, A. *J. Comput. Chem.* **1992**, *13*, 199.
(13) Ten-no, S.; Hirata, F.; Kato, S. *Chem. Phys. Lett.* **1993**, *214*, 391.
(14) Mavri, J.; Berendsen, H. J. C.; Gunsteren, W. F. van. *J. Phys. Chem.* **1993**, *97*, 13469.
(15) Thompson, M. A.; Glendening, E. D.; Feller, D. *J. Phys. Chem.* **1994**, *98*, 10465.
(16) Stanton, R. V.; Hartsough, D. S.; Mertz Jr., K. M. *J. Comput. Chem.* **1995**, *16*, 113.
(17) Vries, A. H. de; Duijnen, P. Th. van; Juffer, A. H.; Rullmann, J. A. C.; Dijkman, J. P.; Merenga, H.; Thole, B. T. *J. Comput. Chem.* **1995**, *16*, 37.
(18) Maseras, F.; Morokuma, K. *J. Comput. Chem.* **1995**, *16*, 1170.
(19) Duijnen, P. Th. van; Vries, A. H. de. *Int. J. Quantum Chem.* **1996**, *60*, 1111.
(20) Bakowies, D.; Thiel, W. *J. Phys. Chem.* **1996**, *100*, 10580.
(21) Eichler, U.; Kölmel, C. M.; Sauer, J. *J. Comput. Chem.* **1997**, *18*, 463.
(22) Kramer, G. J.; Santen, R. A. van; Emeis, C. A.; Novak, A. K. *Nature* **1993**, *363*, 529.
(23) Parillo, D. J.; Gorte, R. J. *J. Phys. Chem.* **1997**, *97*, 8786.
(24) Hill, J. R.; Sauer, J. *J. Phys. Chem.* **1995**, *99*, 9536.
(25) Svensson, M.; Humbel, S.; Froese, R. D. J.; Matsubara, T.; Sieber, S.; Morokuma, K. *J. Phys. Chem.* **1996**, *100*, 19357.
(26) Kramer, G. J.; Santen, R. A. van. *J. Am. Chem. Soc.* **1993**, *115*, 2887.
(27) Nicholas, J. B.; Trouw, F. R.; Mertz, J. E.; Iton, L. E.; Hopfinger, A. J. *J. Phys. Chem.* **1993**, *97*, 4149.
(28) Brooks, B. R.; Bruccoleri, R. E.; Olafson, B. D.; States, D. J.; Swaminathan, S. J.; Karplus, M. *J. Comput. Chem.* **1983**, *4*, 187.
(29) Collins, S. J.; Vries, A. H. de; Sherwood, P.; Greatbanks, S.; Hillier, I. H. Manuscript in preparation.
(30) Baker, J. *J. Comput. Chem.* **1986**, *7*, 385.
(31) Bofill, J. M. *J. Comput. Chem.* **1994**, *15*, 1.
(32) Sherwood, P.; Vries, A. H. de. *ChemShell manual*; Daresbury Laboratories: Daresbury, Warrington WA4 4AD, UK.
(33) GAMESS−UK is a package of ab initio programs written by M. F. Guest, J. H. van Lenthe, J. Kendrick, K. Schoffel, and P. Sherwood, with contributions from R. D. Amos, R. J. Buenker, M. Dupuis, N. C. Handy, I. H. Hillier, P. J. Knowles, V. Bonacic-Koutecky, W. von Niessen, R. J. Harrison, A. P. Rendell, V. R. Saunders, and A. J. Stone. The package is derived from the original GAMESS code due to M. Dupuis, D. Spangler, and J. Wendoloski, NRCC Software Catalog, Vol. 1, Program No. QG01 (GAMESS), 1980.
(34) Smith, W. DL-POLY, DCI, Daresbury Laboratories, Daresbury, Warrington WA4 4AD, UK.
(35) Gallezot, P.; Beaumont, R.; Barthomeuf, D. *J. Phys. Chem.* **1974**, *78*, 155.
(36) Calliaris, M.; Nardin, G.; Randaccio, L. *Acta Crystallogr.* **1982**, *B38*, 602.
(37) Koningsveld, H. van; Bekkum, H. van; Jansen, J. C. *Acta Crystallogr.* **1987**, *B43*, 127.
(38) Olson, D. H.; Kokotailo, G. T.; Lawton, S. L.; Meier, W. M. *J. Phys. Chem.* **1981**, *85*, 2238.
(39) Newsam, J. M.; Treacy, M. M. J.; Koetsier, W. T.; deGruyter, C. B. *Proc. R. Soc. (London) A* **1988**, *420*, 375.
(40) Schlenker, J. L.; Pluth, J. J.; Smith, J. V. *Acta Crystallogr.* **1977**, *B33*, 3265.
(41) Frash, M. V.; Makarova, M. A.; Rigby, A. M. *J. Phys. Chem. B* **1997**, *101*, 2116.
(42) Jirák, Z.; Vratislav, V.; Bosácek, V. *Phys. Chem. Solids* **1980**, *41*, 1089.
(43) Dubský, J.; Beran, S.; Bosácek, V. *J. Mol. Catal.* **1979**, *6*, 321.
(44) Schröder, K.-P.; Sauer, J.; Leslie, M.; Catlow, C. R. A. *Chem. Phys. Lett.* **1992**, *188*, 320.
(45) Sierka, M.; Sauer, J. *Faraday Discuss.* **1997**, *106*, 41.
(46) Schröder, K.-P.; Sauer, J.; Leslie, M.; Catlow, C. R. A. *Zeolites* **1992**, *12*, 20.
(47) Greatbanks, S. P.; Sherwood, P.; Hillier, I. H.; Hall, R. J.; Burton, N. A.; Gould, I. R. *Chem. Phys. Lett.* **1995**, *234*, 367.
(48) Teunissen, E. H.; Duijneveldt, F. B. van; Santen, R. A. van. *J. Phys. Chem.* **1992**, *96*, 366.
(49) Pisani, C.; Birkenheuer, U. *Int. J. Quantum Chem.* **1995**, *S29*, 221.
(50) Greatbanks, S. P.; Hillier, I. H.; Sherwood, P. *J. Comput. Chem.* **1997**, *18*, 562.
(51) Teunissen, E. H.; Roetti, C.; Pisani, C.; Man, A. J. M. de; Jansen, A. P. J.; Orlando, R.; Santen, R. A. van; Dovesi, R. *Mod. Sim. Mater. Sci. Eng.* **1994**, *2*, 921.
(52) Vries, A. H. de; Sherwood, P.; Collins, S. J., manuscript in preparation.
(53) Sherwood, P.; Vries, A. H. de; Collins, S. J.; Greatbanks, S. P.; Burton, N. A.; Vincent, M. A.; Hillier, I. H. *Faraday Discuss.* **1997**, *106*, 79.
(54) Vos-Burghart, E. de; Verheij, V. A.; Bekkum, H. van; Graaf, B. van der. *Zeolites* **1992**, *12*, 183.
(55) MOVIEMOL Version 1.1; Hermansson, K., Ojamäe, L.; Uppsala University, Institute of Chemistry, Report UUIC-B19-500, 1994.